# Double Pile-Up Resonance Energy Harvesting Circuit for Piezoelectric and Thermoelectric Materials

Kye-Seok Yoon, *Student Member, IEEE*, Sung-Wan Hong, and Gyu-Hyeong Cho, *Fellow, IEEE*

***Abstract*— This paper presents a double pile-up resonance energy harvesting circuit that efficiently and simultaneously extracts energy from a piezoelectric transducer (PZT) and a thermoelectric generator. The proposed harvester operates in a double pile-up mode (DPM) to efficiently extract energy from PZT with the enhanced damping force, resulting in a 1452% improvement in power extraction, which is the best performance among the state-of-the-art works. The harvester also operates in a boost converter mode (BCM) without an additional power switch, achieving 75% conversion efficiency at 450-$\mu$W output power. With a single-shared inductor, a simple control scheme enables the harvester to operate in both DPM and BCM by time-multiplexing method, consuming a low quiescent current of 240 nA. The prototype chip fabricated in a 0.18-$\mu$m BCD occupies an area of 1.5 mm × 1 mm, and it was tested with a 20-nF PZT product (PPA-1001) vibrated by a shaker (Type 4810).**

***Index Terms*— Boost mode, double pile-up mode (DPM), energy harvester, piezoelectric transducer (PZT), thermoelectric generator (TEG).**

## I. Introduction

With the development of wireless sensor network, in which thousands of micro-sensor nodes are connected via a wireless network, people are able to accurately monitor a variety of environmental conditions by processing data from individual nodes [1]–[4]. Since most sensors are usually designed with small size, batteries are also small, resulting in quick discharge. Therefore, it is a critical issue to frequently supply power to such a system. However, it is impractical to personally charge or replace the batteries of thousands of individual nodes. One attractive solution is to harvest electrical energy from ambient energy sources such as solar, vibrational, and thermal energy using a photovoltaic cell, a piezoelectric transducer (PZT), and a thermoelectric generator (TEG), respectively. By using energy harvesting techniques, near-perpetual operation of these sensors can be available [5].

Manuscript received August 4, 2017; revised October 17, 2017; accepted November 17, 2017. Date of publication December 20, 2017; date of current version March 23, 2018. This paper was approved by Guest Editor Makoto Ikeda. *(Corresponding author: Sung-Wan Hong.)*

K.-S. Yoon and G.-H. Cho are with the School of Electrical Engineering, Korea Advanced Institute of Science and Technology, Daejeon 34141, South Korea (e-mail: oscar04@kaist.ac.kr; ghcho@kaist.ac.kr).

S.-W. Hong is with the Department of Electronics Engineering, Sookmyung Women's University, Seoul 04310, South Korea (e-mail: hsw0930@sookmyung.ac.kr).

Color versions of one or more of the figures in this paper are available online at http://ieeexplore.ieee.org.

Digital Object Identifier 10.1109/JSSC.2017.2778279

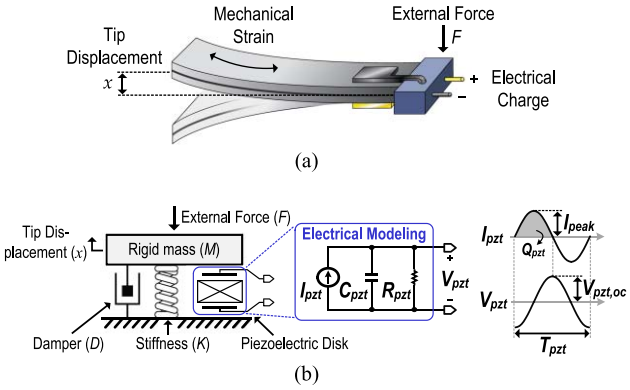


Fig. 1. (a) Operation of cantilever PZT. (b) Equivalent model in an electromechanical domain with associated waveforms.

Among various ambient energy sources mentioned earlier, a number of groups have researched energy harvesting interfaces that extract energy from a cantilever-type PZT [5]–[25], because a PZT can generate relatively high power as much as hundreds of microwatt from the available vibrational energy that exists almost everywhere [26].

Fig. 1(a) illustrates the operation of the cantilever-type PZT. When vibration as an external force ($F$) is applied on to the PZT, mechanical strain develops with the tip displacement ($x$) of the device, resulting in a deformation of the piezoelectric crystal lattice and creating the displacement of the bound charge [12], [18], [19], [22]. In other words, mechanical energy is converted into electrical energy through this transducer: we can obtain electrical energy by harvesting the electrical charge. The equivalent model of the PZT in an electromechanical domain can be represented, as shown in Fig. 1(b). The energy provided by the vibration is divided into kinetic energy, potential elastic energy, mechanical losses, and transferred energy, and is defined as follows [18], [22]:

$$\int F\dot{x}dt = \frac{1}{2}M\dot{x}^2 + \frac{1}{2}Kx^2 + \int D\dot{x}^2 + \int \alpha V_{\text{pzt}}\dot{x}dt \qquad (1)$$

where $M$, $K$, $D$, $\alpha$, and $V_{\text{pzt}}$ are the rigid mass, the global stiffness, the damper, the force factor, and the output port voltage of PZT, respectively. The transferred energy is the part of the mechanical energy that can be converted into electrical energy [18]. When the PZT is excited by sinusoidal vibrations at the resonance frequency, an ac-shaped charge is generated from the piezoelectric disk. Hence, the PZT can

be modeled in an electrical domain as a sinusoidal current source ($I_{\rm pzt}$) in parallel with a parasitic capacitance ($C_{\rm pzt}$) and resistance ($R_{\rm pzt}$). To efficiently extract the transferred energy (or electrical energy) from PZT, it is important to convert more mechanical energy into electrical energy. However, there are two main problems that hinder efficient energy extraction from PZT. One is a considerably large value of $C_{\rm pzt}$ that restricts $I_{\rm pzt}$ from flowing out of PZT. As a result, the charge of PZT cannot be fully extracted. The other problem is an unexpected situation, in which low input vibration excites a PZT. When very little mechanical strain occurs due to low vibration, the electrical energy is rarely generated. Then, energy harvesting from PZT is hard. To complement little energy extraction from PZT, TEG is used together [5], [24]. Practically, energy harvesting system for both PZT and TEG has been applied in the fields of wireless sensor network [27] and human wearable [28]. In addition, commercial evaluated boards are widely used for multiple energy harvesting systems [29], [30].

In this paper, a double pile-up resonance energy harvesting circuit that simultaneously extracts energy from PZT and TEG is proposed. By utilizing *LC* resonance, the proposed harvester can fully extract the charge from PZT. In addition, TEG is utilized with the PZT to extract sufficient power, even in situations with low input vibration. By using a double pile-up resonance technique to increase $V_{\rm pzt}$, the proposed harvester can efficiently convert sufficient mechanical energy into electrical energy. Consequently, compared to a full-bridge rectifier, the proposed structure achieves high improvement of power extraction, when using only the PZT. For energy extraction from the TEG, the proposed harvester can operate as a boost converter without additional power switches. Since a core structure with a single inductor is shared and used to extract the energy from both energy sources, the circuit complexity is reduced while consuming low quiescent current. This paper is organized as follows. In Section II, previous approaches to piezoelectric energy harvesting are discussed. The concept to the proposed harvester is explained and analyzed in Section III. The circuit implementation is described in Section IV. Measurement results for the prototype chip and a performance comparison are presented in Section V. A brief conclusion is provided in Section VI.

## II. Previous Approaches to Piezoelectric Energy Harvesting

Before analyzing the previous approaches that have been used to extract electrical energy from PZT, we discuss the basic characteristics of PZT in an electrical domain. For the following analysis, the input vibration is assumed to be sinusoidal in nature and $R_{\rm pzt}$ is ignored due to its quite large value of several megaohm [17]. With these assumptions, voltage and current waveforms of an open circuit of PZT are shown at the right of Fig. 1(b). $I_{\rm pzt}$ is generated as a sine-waveform, and is given by

$$I_{\rm pzt} = I_{\rm peak}\sin(2\pi f_{\rm pzt}t) \tag{2}$$

where $I_{\rm peak}$ is the magnitude of $I_{\rm pzt}$ and is proportional to the amplitude of the input vibration, and $f_{\rm pzt}$ is a resonant frequency of PZT. The time of one cycle of PZT ($T_{\rm pzt}$) is the inverse of $f_{\rm pzt}$. The magnitude of $V_{\rm pzt}$ in the open circuit ($V_{\rm pzt,oc}$) can be defined as follows:

$$V_{\rm pzt,oc} = \frac{1}{C_{\rm pzt}}\int_{T_{\rm pzt}/4}^{T_{\rm pzt}/2} I_{\rm pzt}dt = \frac{I_{\rm peak}}{2\pi f_{\rm pzt}C_{\rm pzt}}. \tag{3}$$

From (3), the charge on the half cycle ($Q_{\rm pzt}$) can be defined as follows:

$$Q_{\rm pzt} = C_{\rm pzt}\cdot 2V_{\rm pzt,oc} = \frac{I_{\rm peak}}{\pi f_{\rm pzt}}. \tag{4}$$

According to (4), $Q_{\rm pzt}$ is related to both the vibration and the resonant frequency of PZT. In other words, an absolute quantity of energy extraction depends on the external environmental conditions. Since we cannot control the external conditions, it is important to design an energy harvester that extracts more electrical energy under the same conditions.

In this section, we discuss previous approaches to piezoelectric energy harvesting. For an intuitive analysis, it is assumed that the parasitic resistance of the components and the forward voltage drop of the diode are negligible.

Because of its simplicity, a full-bridge rectifier (FBR) is conventionally used to convert the ac output of PZT into a dc voltage [6]. To extract the charge from PZT in the FBR, the magnitude of $V_{\rm pzt}$ should be higher than the voltage of the battery ($V_{\rm bat}$) in order to conduct the diodes. When the polarity of $I_{\rm pzt}$ changes in FBR, some charge of the PZT should be used to flip $V_{\rm pzt}$ by as much as $2V_{\rm bat}$. Since the amount of this charge on the half cycle cannot be extracted to the battery, it is called a loss charge ($Q_{\rm loss} = 2C_{\rm pzt}\cdot V_{\rm bat}$) [10]. From (4), the average extracted power in the FBR ($P_{\rm FBR}$) is calculated as

$$\begin{aligned} P_{FBR} &= (Q_{\rm pzt} - Q_{\rm loss})\cdot V_{\rm bat}\cdot 2f_{\rm pzt} \\ &= 4C_{\rm pzt}\cdot(V_{\rm pzt,oc} - V_{\rm bat})\cdot V_{\rm bat}\cdot f_{\rm pzt}. \end{aligned} \tag{5}$$

From (5), the maximum power of FBR ($P_{\rm FBR,max}$) can be obtained when $V_{\rm bat}$ becomes $V_{\rm pzt,oc}/2$, and is given by [6]

$$P_{FBR,\max} = C_{\rm pzt}\cdot f_{\rm pzt}\cdot V_{\rm pzt,oc}^2 = \frac{I_{\rm peak}^2}{4\pi^2 f_{\rm pzt}\cdot C_{\rm pzt}}. \tag{6}$$

Since $I_{\rm peak}$ and $f_{\rm pzt}$ are determined by the input vibration and the characteristics of the PZT, which cannot be controlled, it is important to choose a PZT that has sufficiently low $C_{\rm pzt}$ to reduce $Q_{\rm Loss}$. However, most products of PZT have a large value of $C_{\rm pzt}$ (as high as several nanofarad) [8], [14], [15]. Therefore, energy extraction from the PZT using FBR is not efficient.

To minimize $Q_{\rm loss}$ in FBR, a bias-flip rectifier, shown in Fig. 2(a), was reported in [6]. When the polarity of $I_{\rm pzt}$ changes, *LC* resonance is induced by the instant switch operation. As a result, $V_{\rm pzt}$ can be flipped to $2V_{\rm bat}$ without using the charge of the PZT, as shown in Fig. 3(a). In an ideal case, $Q_{\rm loss}$ can be completely ignored. Hence, the extracted power on average in the bias flip ($P_{\rm BF}$) can be defined as follows:

$$P_{BF} = Q_{\rm pzt}\cdot V_{\rm bat}\cdot 2f_{\rm pzt} = 4C_{\rm pzt}\cdot V_{\rm pzt,oc}\cdot V_{\rm bat}\cdot f_{\rm pzt}. \tag{7}$$

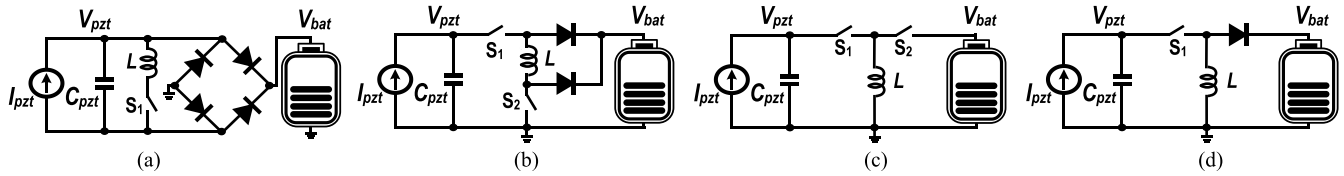


Fig. 2. Piezoelectric energy harvesters. (a) Bias-flip rectifier [6]. (b) Rectifier-less structure [13]. (c) Investment structure [17]. (d) Pile-up structure [23].

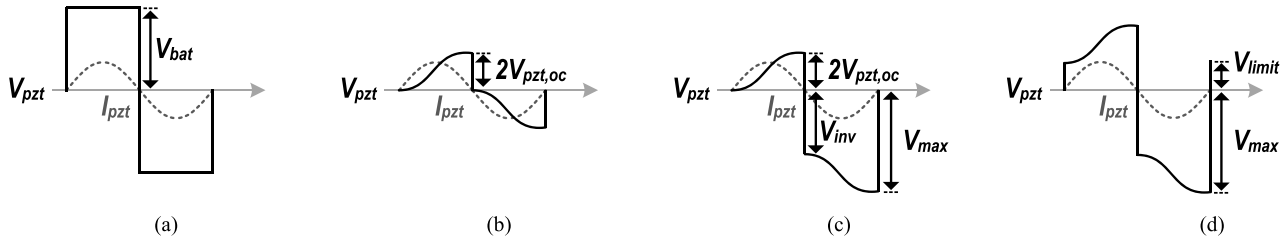


Fig. 3. Associated waveforms. (a) Bias-flip rectifier [6]. (b) Rectifier-less structure [13]. (c) Investment structure [17]. (d) Pile-up Structure [23].

Comparing (7) with (5), the bias-flip rectifier can obtain the extracted power from the PZT more than the FBR, by eliminating $Q_{\text{loss}}$. However, since $P_{\text{BF}}$ is proportional to a level of $V_{\text{bat}}$, energy harvesting using the bias-flip rectifier is not efficient at low $V_{\text{bat}}$.

The rectifier-less structure shown in Fig. 2(b) was proposed to eliminate the need for a rectifier core and increase the electrical damping in [13]. The damping in physics means restraining of the vibratory motion by dissipation of energy. Interestingly, when the higher voltage is applied to the terminal of PZT, more electrical power can be extracted. This is because the damping force is enhanced by applying higher voltage. In other words, a certain fraction of more mechanical energy is converted into electrical energy by the enhanced damping force, which is caused by intentionally applying the higher voltage to PZT [17]. By storing $Q_{\text{pzt}}$ in $C_{\text{pzt}}$, the rectifier-less harvester increases the value of $V_{\text{pzt}}$ up to $2V_{\text{pzt,oc}}$ during the half cycle of $I_{\text{pzt}}$, as shown in Fig. 3(b). When the polarity of $I_{\text{pzt}}$ changes, all the energy stored in $C_{\text{pzt}}$ is transferred to the battery by utilizing an inductor. Hence, the extracted power on average in the rectifier-less structure ($P_{\text{RL}}$) can be defined as follows:

$$P_{RL} = \frac{1}{2} C_{\text{pzt}} \cdot (2V_{\text{pzt,oc}})^2 \cdot 2f_{\text{pzt}} = 4C_{\text{pzt}} \cdot f_{\text{pzt}} \cdot V_{\text{pzt,oc}}^2. \tag{8}$$

Comparing (8) with (6), theoretically, the rectifier-less harvester can extract four times more average power than the FBR, regardless of the level of $V_{\text{bat}}$. Even when $V_{\text{pzt,oc}}$ is lower than $V_{\text{bat}}$, energy extraction is available because energy is transferred to the battery in the form of current by using the inductor. In [13], a 290-nF PZT was used, and it was activated at the operating frequency of 100 Hz. Although the rectifier-less structure obtained the output power of 30 $\mu$W at $V_{\text{pzt,oc}}$ of 1.2 V, it hardly extracted the power from PZT in the case of a relatively low $V_{\text{pzt,oc}}$. This is because $V_{\text{pzt}}$ cannot be increased over $2V_{\text{pzt,oc}}$ in the rectifier-less structure.

To extract more potential energy from the PZT, the investment structure shown in Fig. 2(c) was proposed in [17]. As shown in Fig. 3(c), this concept is related to the use of the energy of the battery being invested to further increase the magnitude of $V_{\text{pzt}}$ to $V_{\text{inv}}$ at the point of half cycle of $I_{\text{pzt}}$; then, the energy stored in $C_{\text{pzt}}$ is transferred to the battery at the end cycle of $I_{\text{pzt}}$. By adopting this technique, more electrical energy can be obtained. This is because the linear increment of $V_{\text{pzt}}$ in $C_{\text{pzt}}$ produces quadratic increments of the energy in $C_{\text{pzt}}$ [17]. By subtracting all the energy stored in $C_{\text{pzt}}$ from the energy invested from the battery, the practically extracted power on average in the investment structure ($P_{\text{inv}}$) can be calculated as follows:

$$\begin{aligned} P_{inv} &= \left(\frac{1}{2} C_{\text{pzt}} \cdot V_{\text{max}}^2 - \frac{1}{2} C_{\text{pzt}} \cdot \left(V_{inv}^2 - (2V_{\text{pzt,oc}})^2\right)\right) \cdot f_{\text{pzt}} \\ &= 2C_{\text{pzt}} \cdot V_{\text{pzt,oc}} \cdot V_{\text{max}} \cdot f_{\text{pzt}} \end{aligned} \tag{9}$$

where $V_{\text{max}}$ is the maximum voltage of $V_{\text{pzt}}$. In the investment structure, $V_{\text{max}}$ is the sum of $V_{\text{inv}}$ and $2V_{\text{pzt,oc}}$. According to (9), more energy can be extracted, as $V_{\text{max}}$ is further increased by investing more energy from the battery. However, $V_{\text{max}}$ should be considered to determine whether it has deadly effects on the harvester circuit for high voltage stress. In [17], a 15-nF PZT was used, and it was vibrated at the frequency of 143 Hz. The investment structure obtained 52 $\mu$W at $V_{\text{pzt,oc}}$ of 2.6 V, which was 3.51 times more power than the maximum power of FBR from (6). Although more electrical energy from the PZT can be extracted by enhancing the damping force, using the energy of the battery is somewhat inefficient.

To increase $V_{\text{pzt}}$ without using any energy from the battery, a pile-up structure, shown in Fig. 2(d), was reported in [23]. The concept is that $V_{\text{pzt}}$ is increased to a limited voltage ($V_{\text{limit}}$) by the self-energy of the PZT; then, the energy stored in $C_{\text{pzt}}$ is harvested at the end of the period, as shown in Fig. 3(d). Therefore, the pile-up structure can obtain more electrical energy as well. By subtracting all the energy stored in $C_{\text{pzt}}$ from the energy used to increase $V_{\text{pzt}}$ to $V_{\text{limit}}$, the practically extracted power on average in the pile-up structure ($P_{\text{pile}}$) can be defined as follows:

$$\begin{aligned} P_{pile} &= \left(\frac{1}{2} C_{\text{pzt}} \cdot \left(V_{\text{max}}^2 - V_{limit}^2\right)\right) \cdot f_{\text{pzt}} \\ &= 4C_{\text{pzt}} \cdot V_{\text{pzt,oc}} \cdot (V_{\text{max}} - 2V_{\text{pzt,oc}}) \cdot f_{\text{pzt}}. \end{aligned} \tag{10}$$

In the pile-up structure, $V_{max}$ is the sum of $V_{limit}$ and 4 $V_{pzt,oc}$. Similar to the investment structure, $V_{max}$ is designed not to be too high for the voltage stress in the pile-up structure. In [23], a 220-nF PZT was used, and it operated at the frequency of 100 Hz. The pile-up structure obtained 87 $\mu$W at $V_{pzt,oc}$ of 0.65 V, which was 9.36 times more power than the maximum power of FBR from (6). Although more electrical energy can be obtained by increasing $V_{pzt}$ with the self-energy of the PZT, it is inefficient that energy extraction take place just once every period of $I_{pzt}$.

## III. Proposed Energy Harvesting Circuit

As mentioned earlier, many previous approaches have been proposed to efficiently extract the energy from the PZT by eliminating $Q_{loss}$ or strengthening the damping force. Nevertheless, there is still room for more power from the PZT. This section presents a topology of the proposed piezoelectric energy harvester, and proves that the proposed structure can improves the power extraction capability from PZT more than the previous works through quantitative analysis. Also, it shows that the proposed harvester is capable of simultaneous energy extraction from another energy source, TEG, without additional power switches.

### A. Concept and Operation

The simplified structures of the proposed piezoelectric energy harvesters without TEG and with TEG are shown in Fig. 4(a) and (b), respectively. The power stage is composed of four main switches (SW1–SW4), an active diode (AD), and an inductor ($L_{ind}$). The proposed double pile-up resonance energy harvesting circuit can operate in two modes; a double pile-up mode (DPM) and a boost converter mode (BCM). The purpose of DPM is to efficiently increase the magnitude of $V_{pzt}$ to extract more electrical energy from PZT. Also, when both PZT and TEG exist for the case of Fig. 4(b), the proposed harvester operating in DPM can simultaneously extract energy from both the PZT and the TEG. The purpose of BCM is to mainly extract the energy from the TEG. Fig. 4(c) shows an overall timing diagram of the proposed structure. The operation sequence of DPM is as follows. During the first positive half-cycle of $I_{pzt}$, $V_{pzt}$ increases to $2V_{pzt,oc}$. At the first zero crossing point of $I_{pzt}$, the $LC$ resonance begins and is maintained to flip $V_{pzt}$ during half of the $LC$ resonance time $T_{res}$ ($= \pi(L_{ind}C_{pzt})^{1/2}$). This step is called a bias-flip phase ($\Phi_{BF}$). If TEG does not exist, $V_{pzt}$ is flipped as much as a magnitude of $V_{pzt}$ ($= 2V_{pzt,oc}$). Otherwise, $V_{pzt}$ is more flipped because the energy of TEG is additionally transferred to the current of inductor ($I_{ind}$). After $\Phi_{BF}$, the magnitude of $V_{pzt}$ starts to increase again during the negative half-cycle of $I_{pzt}$. Likewise, $V_{pzt}$ is flipped again at the second zero crossing point of $I_{pzt}$. If this process is repeated for a few cycles, the swing of $V_{pzt}$ continuously grows; the rate of the growth is determined by the state of TEG (or $V_{teg}$). Although the larger damping force caused by the higher $V_{pzt}$ enables more mechanical energy to be converted into electrical energy, the magnitude of $V_{pzt}$ is limited to a preset initial voltage ($V_{init}$) to prevent the harvesting circuit from incurring high voltage stress. When the magnitude of $V_{pzt}$ reaches $V_{init}$ during the

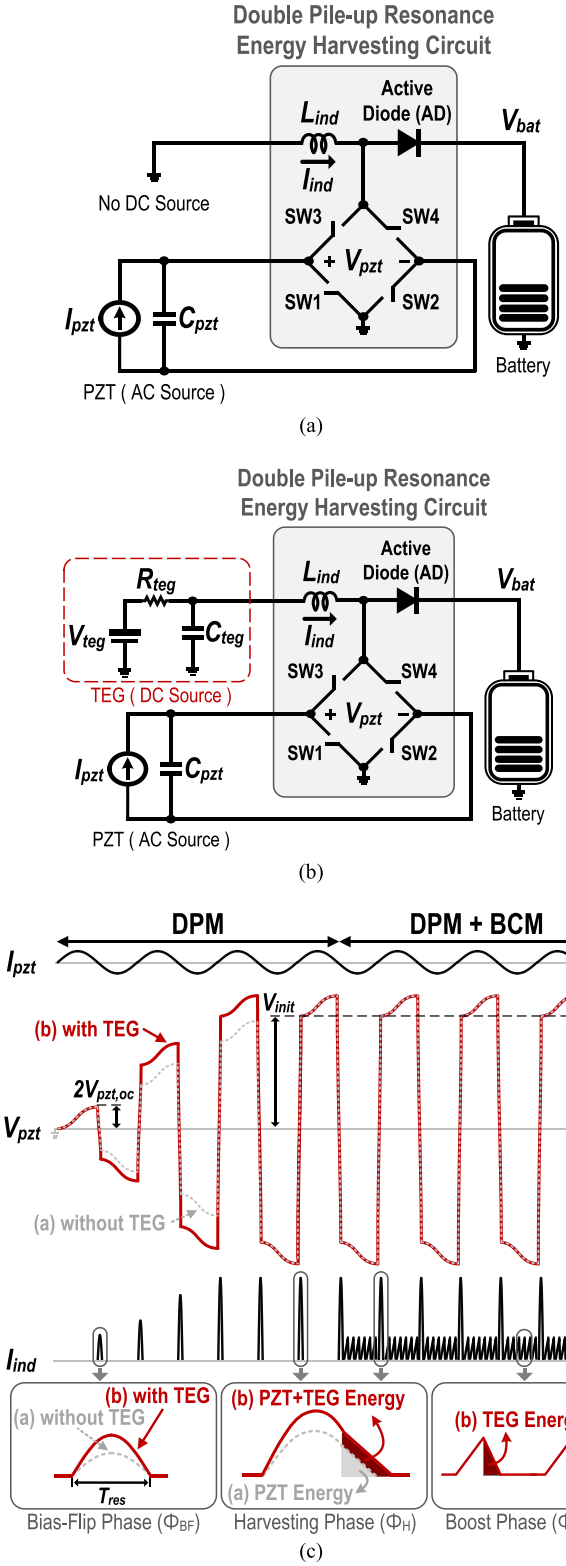


Fig. 4. Simplified proposed piezoelectric energy harvester. (a) Without TEG. (b) With TEG. (c) Overall timing diagrams.

$LC$ resonance, the proposed harvester stops the $LC$ resonance; then, it transfers the residual energy in $L_{ind}$ to the battery through AD. This step is called the harvesting phase ($\Phi_H$). Similarly, the amount of extracted energy depends on $V_{teg}$.

Fig. 5 shows the power switch configurations in DPM with associated voltage and current waveforms in detail, when both

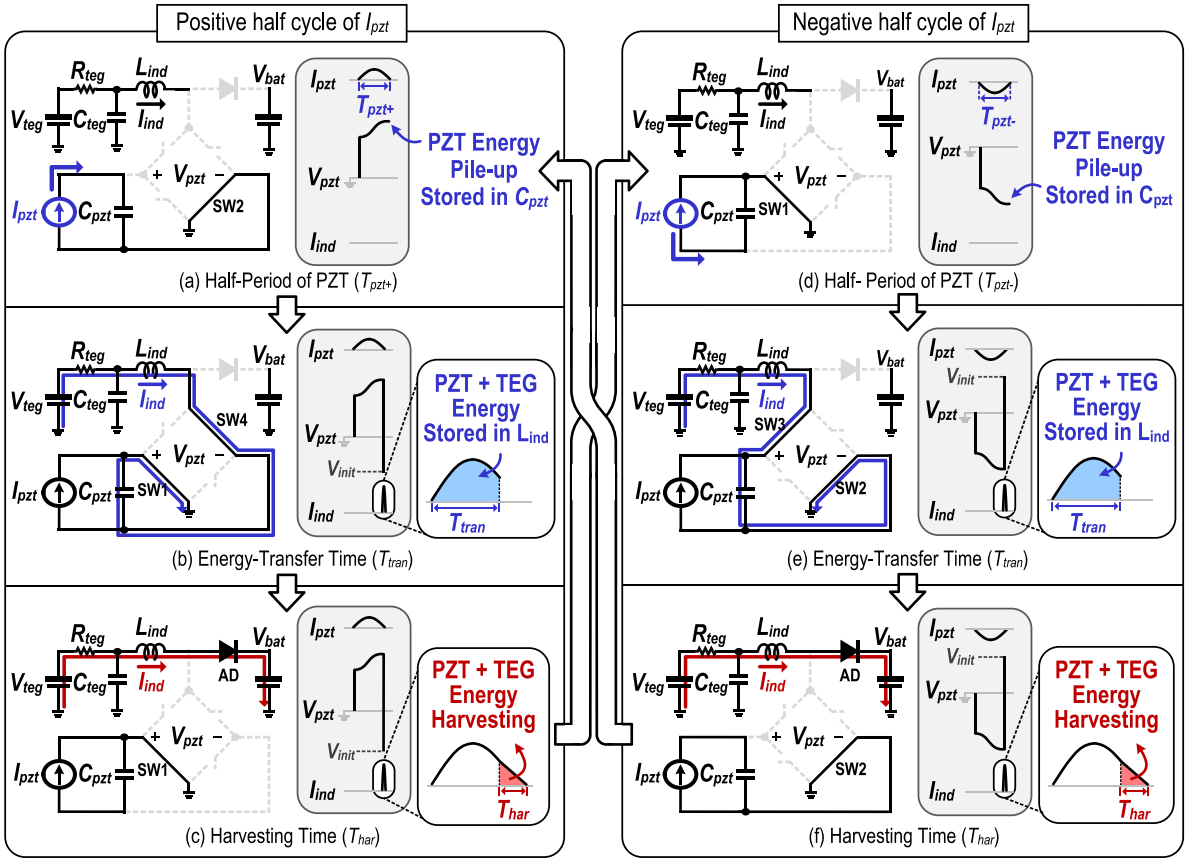


Fig. 5. Power switch configurations in DPM with associated voltage and current waveforms.

PZT and TEG are available. The steady-state operation of the positive half cycle of $I_{\rm pzt}$ corresponds to Fig. 5(a)–(c) and that of negative half cycle to Fig. 5(d)–(f). During the positive half cycle, $I_{\rm pzt}$ flows to $C_{\rm pzt}$ to pile-up $V_{\rm pzt}$ by turning on SW2, as shown in Fig. 5(a). When $I_{\rm pzt}$ reaches zero, resonance begins between $L_{\rm ind}$ and $C_{\rm pzt}$ by turning on SW1 and SW4, as shown in Fig. 5(b). As a result, both the energy of the PZT stored in $C_{\rm pzt}$ and that of the TEG in $C_{\rm teg}$ are simultaneously transferred to $L_{\rm ind}$. Then, the energy stored in $L_{\rm ind}$ is used to flip $V_{\rm pzt}$ to the level of $V_{\rm init}$. This duration is called the energy transfer time $T_{\rm tran}$. After $T_{\rm tran}$, the residual energy stored in $L_{\rm ind}$ is transferred to the battery through AD, until $I_{\rm ind}$ becomes zero, as shown in Fig. 5(c). This duration is called the harvesting time $T_{\rm har}$. In the case of the negative half cycle, the process works on the same principle except for the switch configuration, as can be seen in Fig. 5(d)–(f).

In BCM, the proposed harvester operates as a boost converter. Since the PZT is normally excited at hundreds of Hertz, the harvester in BCM can operate at several kilos of Hertz between the edges of $I_{\rm pzt}$. This step is called the boost phase ($\Phi_{\rm bst}$), as shown in Fig. 4(c). Therefore, by adopting a time-multiplexing method, the proposed harvester can independently operate in both DPM and BCM to extract energy from both the PZT and the TEG. Fig. 6 shows the power switch configurations in BCM with the associated waveforms in detail. The steady-state operation of the positive half cycle of $I_{\rm pzt}$ corresponds to Fig. 6(a) and (b), and that of the negative half cycle to Fig. 6(c) and (d). During the positive half cycle, the energy of TEG is transferred to $L_{\rm ind}$ by turning on both the SW2 and SW4, as shown in Fig. 6(a). This duration is called the inductor current build-up time $T_D$. After $T_D$, the energy stored in $L_{\rm ind}$ is transferred to the battery through AD during the harvesting time $T_{\rm har}$, as shown in Fig. 6(b). Likewise, the process works on the same principle with the opposite switch configuration in the case of the negative half cycle, as can be seen in Fig. 6 (c) and (d).

The proposed scheme may look similar to that in [23] in the respect that $V_{\rm pzt}$ piles up cycle-by-cycle and the residual energy in $L_{\rm ind}$ is transferred to the battery. In [23], however, the energy of the TEG cannot be transferred to $L_{\rm ind}$ during the *LC* resonance. Therefore, it is impossible to extract the energy from the TEG, unless the boost converter is used. Even without a TEG, the proposed structure can extract more energy than that in [23], because the direction of $I_{\rm ind}$ is always positive after the *LC* resonance, regardless of the polarity of $I_{\rm pzt}$. As a result, energy extraction can take place twice in one cycle, which was not possible in [23] (The detailed analysis of energy extraction will be discussed in the following part).

### *B. Analysis of Power Extraction*

For quantitative analysis of the power extracted from the PZT by using the proposed structure, the associated waveforms in one period are depicted in Fig. 7. Since the extracted power depends on the existence of the TEG, we will analyze each case separately.

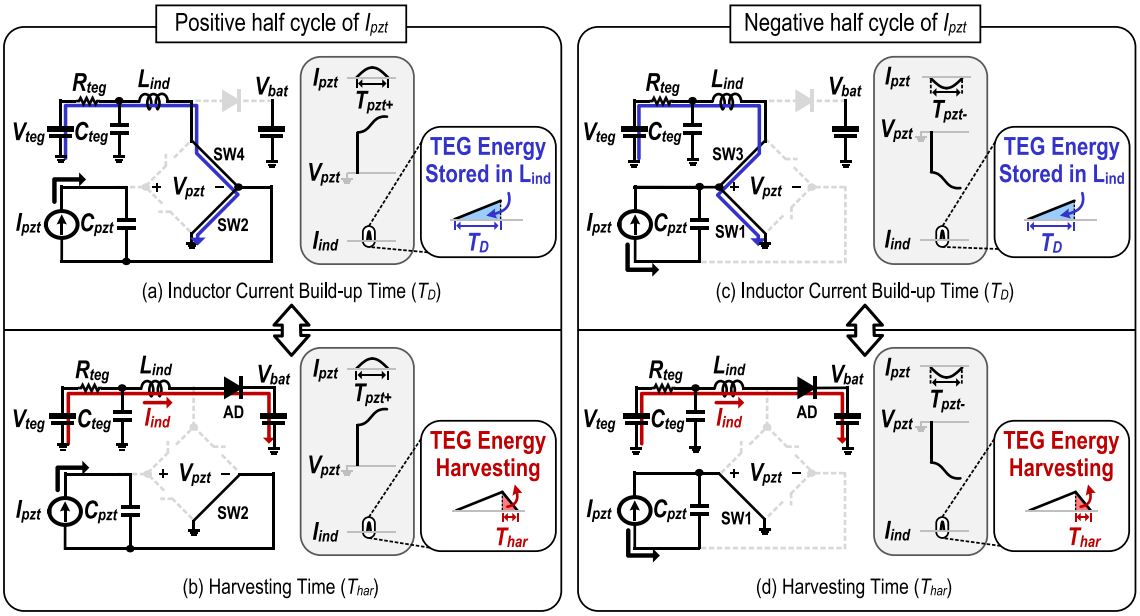


Fig. 6. Power switch configurations in BCM with associated voltage and current waveforms.

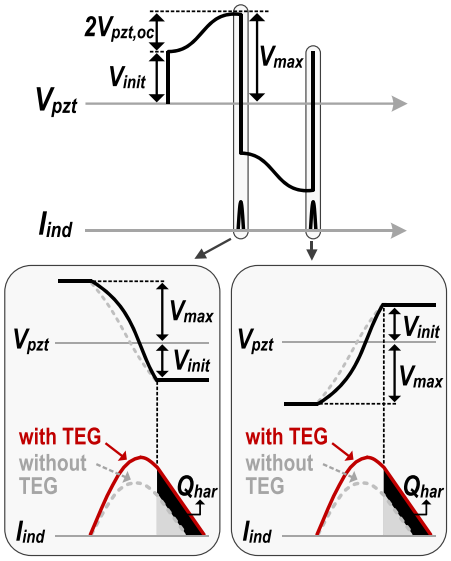


Fig. 7. Operating waveforms without and with TEG in a period.

*1) Extracted Power on Average Without TEG:* First, we discuss how much our harvester operating in DPM extracts the power from PZT in one cycle, as can be seen in Fig. 4(a). At the beginning of the period, $V_{\text{pzt}}$ starts rising from $V_{\text{init}}$ to the maximum voltage ($V_{\text{max}}$). $V_{\text{max}}$ is the sum of $V_{\text{init}}$ and $2V_{\text{pzt,oc}}$ in the proposed structure, given the assumption that all the charges on the half cycle are integrated to $C_{\text{pzt}}$. The proposed harvester uses some parts of the energy stored in $C_{\text{pzt}}$ to flip the magnitude of $V_{\text{pzt}}$ to a value as high as $V_{\text{int}}$; harvester then utilizes $L_{\text{ind}}$ to extract the rest of the energy in $C_{\text{pzt}}$. Thus, the energy extracted by the proposed structure without TEG ($E_{\text{pro,noTEG}}$) is given by

$$E_{\text{pro,noTEG}} = \frac{1}{2}C_{\text{pzt}} \cdot (V_{\text{max}}^2 - V_{\text{init}}^2) = 2C_{\text{pzt}} \cdot V_{\text{pzt,oc}} \cdot (V_{\text{max}} - V_{\text{pzt,oc}}) \quad (11)$$

with

$$V_{\text{init}} = V_{\text{max}} - 2V_{\text{pzt,oc}}. \quad (12)$$

Since the energy extraction is conducted twice in one cycle, the extracted power on average ($P_{\text{pro,noTEG}}$) is defined as follows:

$$P_{\text{pro,noTEG}} = E_{\text{pro,noTEG}} \cdot 2f_{\text{pzt}} = 4C_{\text{pzt}} \cdot V_{\text{pzt,oc}} \cdot (V_{\text{max}} - V_{\text{pzt,oc}}) \cdot f_{\text{pzt}}. \quad (13)$$

For fair comparison of the extracted power on average among various energy harvesters, the external environmental condition and the PZT device are assumed to be in the same condition that $V_{\text{oc,pzt}}$, $V_{\text{max}}$, $C_{\text{pzt}}$, and $f_{\text{pzt}}$ are 1.2 V, 7 V, 20 nF, and 140 Hz, respectively. Fig. 8 shows a graph of the extracted power for various energy harvesters on average in theory with varying $V_{\text{bat}}$. According to (6), theoretically, the maximum extracted power of FBR is 4 $\mu$W at the $V_{\text{bat}}$ of 0.6 V. Meanwhile, other structures using the inductor are not affected by the level of $V_{\text{bat}}$. From (8), the rectifier-less structure of Fig. 2(b) can obtain 16.1 $\mu$W in theory, which is quite low due to low $V_{\text{pzt}}$ of 0.6 V. From (9) and (10), the investment structure of Fig. 2(c) and the pile-up structure of Fig. 2(d) can ideally extract 47 and 61.8 $\mu$W, respectively. Likewise, the proposed harvester can achieve a value of 77.9 $\mu$W from (13). In comparison of the theoretically extracted power, the proposed structure can achieve power extraction capability of 1947% more than the FBR in the ideal case. So far, the proposed harvester can extract the highest extracted power from PZT under the same conditions among [13], [17], and [23], as can be seen in Fig. 8. This is because more mechanical energy is able to be converted into electrical energy by efficiently increasing $V_{\text{pzt}}$.

*2) Extracted Power on Average With TEG:* Now, we discuss how much our harvester operating in DPM extracts the power from both PZT and TEG in one cycle, as can be seen in

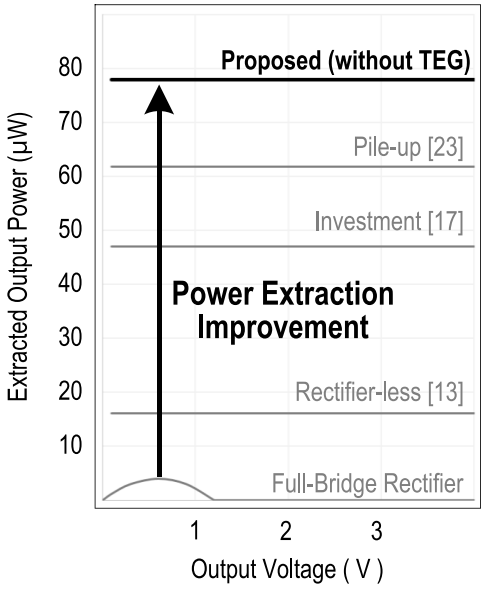


Fig. 8. Graphs of the extracted power for various energy harvesters on average in theory.

Fig. 4(b). Although the presence (or absence) of TEG does not affect the operation of the proposed harvester, the amount of extracted energy highly depends on the $V_{\text{teg}}$. When the magnitude of $V_{\text{pzt}}$ is flipped from $V_{\max}$ to $V_{\text{init}}$, not only the energy stored in $C_{\text{pzt}}$ but also the energy from TEG is transferred to $L_{\text{ind}}$. Thus, the energy stored in $L_{\text{ind}}$ ($E_{\text{ind}}$) is defined as follows:

$$E_{\text{ind}} = \frac{1}{2} L_{\text{ind}} \cdot I_{\text{ind}}^2 = \frac{1}{2} C_{\text{pzt}} \cdot \left(V_{\max}^2 - V_{\text{init}}^2\right) + C_{\text{pzt}} \cdot (V_{\max} + V_{\text{init}}) \cdot V_{\text{teg}}. \tag{14}$$

From (14), the magnitude of the square of $I_{\text{ind}}$ can be modified as follows:

$$I_{\text{ind}}^2 = \frac{1}{L_{\text{ind}}} C_{\text{pzt}} \cdot \left(V_{\max}^2 - V_{\text{init}}^2 + 2(V_{\max} + V_{\text{init}}) \cdot V_{\text{teg}}\right). \tag{15}$$

From (15), the harvested charge ($Q_{\text{har}}$) shown in Fig. 7 is defined as follows:

$$Q_{\text{har}} = \frac{1}{2} \frac{L_{\text{ind}}}{V_{\text{bat}} - V_{\text{teg}}} I_{\text{ind}}^2 = \frac{1}{2(V_{\text{bat}} - V_{\text{teg}})} \cdot C_{\text{pzt}} \cdot \left(V_{\max}^2 - V_{\text{init}}^2 + 2(V_{\max} + V_{\text{init}}) \cdot V_{\text{teg}}\right). \tag{16}$$

As a result, the energy extracted by the proposed structure with TEG ($E_{\text{pro,TEG}}$) is finally defined as follows:

$$E_{\text{pro,TEG}} = Q_{\text{har}} \cdot V_{\text{bat}} = \frac{V_{\text{bat}}}{2(V_{\text{bat}} - V_{\text{teg}})} \cdot C_{\text{pzt}} \cdot \left(V_{\max}^2 - V_{\text{init}}^2 + 2(V_{\max} + V_{\text{init}}) \cdot V_{\text{teg}}\right). \tag{17}$$

For the proposed structure, the ratio of the extracted energy without TEG as given by (13) to that with TEG can be given by

$$\frac{E_{\text{pro,TEG}}}{E_{\text{pro,noTEG}}} = \frac{V_{\text{bat}}}{V_{\text{bat}} - V_{\text{teg}}} \cdot \left(1 + \frac{V_{\text{teg}}}{V_{\max} + V_{\text{init}}}\right). \tag{18}$$

According to (18), it is clear that more energy from TEG can be extracted as $V_{\text{teg}}$ increases.

The proposed harvester can be easily applicable to other energy sources that can be modeled as dc voltage sources as well as TEG. Furthermore, owing to the high flexibility of our energy harvester topology, different types of energy sources, such as ac current sources and dc voltage sources, can be simultaneously and efficiently extracted with a single inductor. Therefore, the proposed energy harvesting circuit configuration can be suitable for multiple energy source harvester.

## IV. Circuit Implementation

Fig. 9(a) shows a block diagram of the proposed harvester. Low-side power switches of SW1–SW2 are implemented as n-type MOSFETs ($M_{\text{sw1}-2}$). High-side power switches of SW3–SW4 and AD are implemented as p-type MOSFETs ($M_{\text{sw3}-4}$, and $M_{\text{AD}}$). Since the operating frequency of the low-side switches is related to the frequency of DPM, which is quite low such as hundreds of hertz, the size of the low-side switches was chosen as large as possible in order to reduce the parasitic resistance. On the other hand, the operating frequency of the high-side switches is related to the frequency of BCM, which is quite high such as several kilohertz. Thus, the size of the high-side switches should be designed smaller than the low-side switches with considering both switching loss and conduction loss. Freewheeling switch ($M_{\text{fw}}$) is used to prevent fluctuation of the switching node ($V_X$), when $M_{\text{sw3}-4}$ and AD are all off.

During $T_{\text{tran}}$, each node voltage of $V_{\text{pzt}}$ ($V_{\text{pzt}+}$ or $V_{\text{pzt}-}$) greatly drops to $-V_{\max}$. Then, if the substrate voltage of low-side switches is not lower than $-V_{\max}$, the body diode of low-side switches can be forward-biased, which is not an unwanted situation. In [17], an externally negative voltage supply was used to solve this problem, but the use of additional supply can be burdensome. Therefore, we adopted a body-bias switching technique with a negative-swing gate driver (NGD), as shown in Fig. 9(b). NGD is divided into $\text{NGD}_{\text{p}}$ for p-type power switches and $\text{NGD}_{\text{n}}$ for n-type power switches, which are determined by presence or absence of an inverter logic gate (INV). By using a flying capacitor ($C_{\text{fly}}$) charged by $V_{\text{bat}}$, a voltage of the gate of SW1–SW4 ($V_{g1-4}$) can drop to $-V_{\text{bat}}$. Thus, the body diodes of low-side switches cannot operate in a forward-bias region, and all of the power switches can be fully switched ON and OFF without using a negative power supply. However, since the use of this gate driver limits the level of $V_{\max}$ to the level of $V_{\text{bat}}$, the level of $V_{\text{pzt}}$ cannot be increased over the level of $V_{\text{bat}}$. Therefore, the power extraction performance could not be enough at the low $V_{\text{bat}}$. Even though performance at low $V_{\text{bat}}$ can be improved by using the negative power supply [17], this power supply much increases a complexity of the system. Considering the system complexity, this negative gate driver is more efficient. Moreover, the performance is getting better as the $V_{\text{bat}}$ increase.

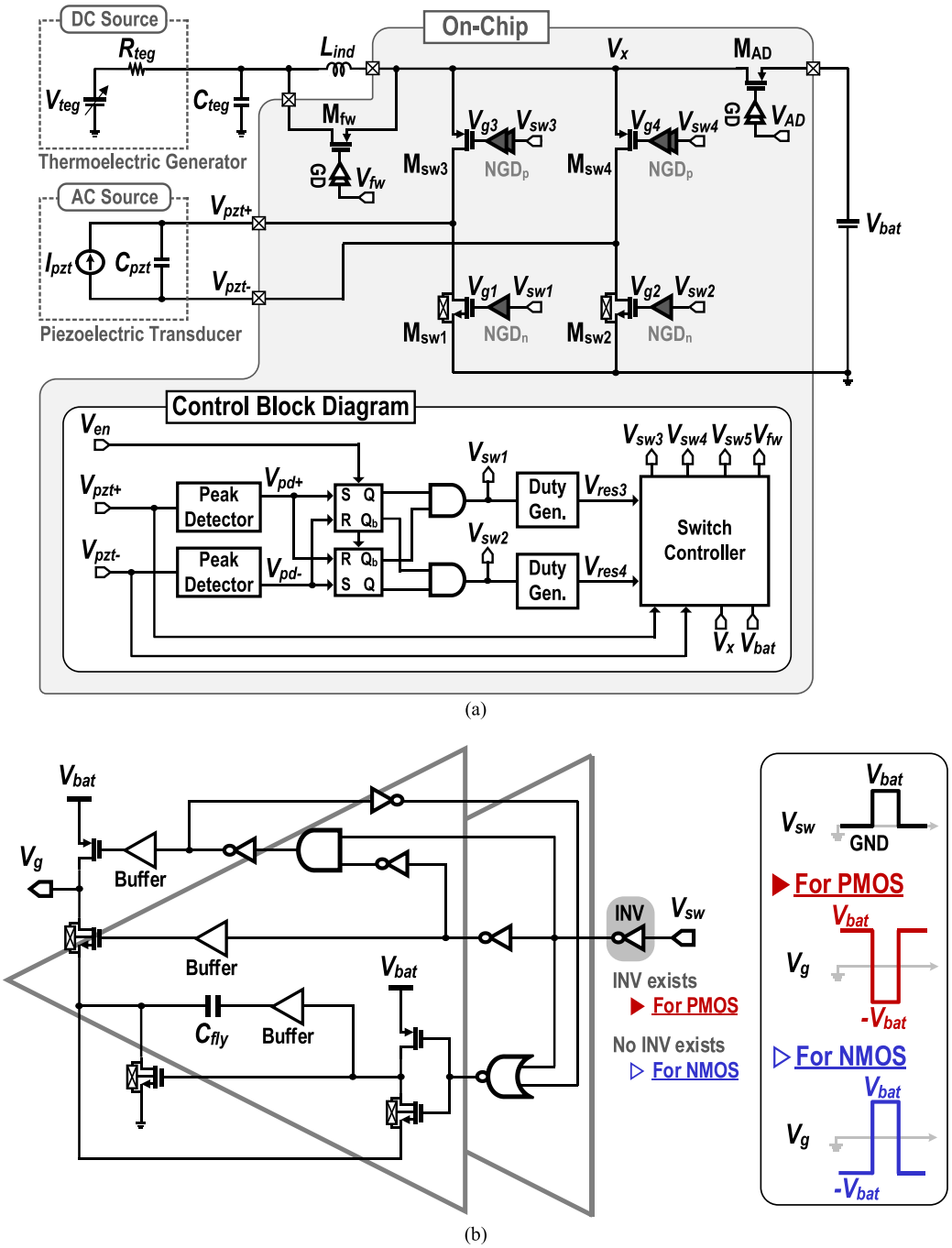


Fig. 9. (a) Overall block diagram of the proposed energy harvesting circuit. (b) NGD.

For the operation of DPM and BCM, the proposed harvester is required to detect the zero crossing point of $I_{\rm pzt}$, generate the duty of $T_{\rm res}$, and control the sequence of the switch operation. Fig. 10 shows each control block diagram of the proposed harvester in detail. Normally, since the zero current sensing circuit is complicated and consumes relatively large power, we detect a peak of $V_{\rm pzt}$, which implies the zero current of $I_{\rm pzt}$, as can be seen in Fig. 10(a). With the *RC* delay filter and the comparator, the short pulse of the peak signal ($V_{\rm pd+,-}$) can be generated simply by comparing $V_{\rm pzt+,-}$ with the *RC* delay signal ($V_{\rm dly}$) [13]. To minimize the quiescent current of the peak detector, a latched comparator operating with a low-frequency clock of 10 kHz is adopted. To implement the *LC* resonance duration $T_{\rm res}$, we used a duty generator that generates the resonance duty signal $V_{\rm res3}$ (or $V_{\rm res4}$) at every falling edge of $V_{\rm sw1}$ (or $V_{\rm sw2}$), as shown in Fig. 10(b). At the falling edge of $V_{\rm sw1}$ (or $V_{\rm sw2}$), $V_{\rm res3}$ (or $V_{\rm res4}$) becomes high until an integrated signal ($V_{\rm dg}$) reaches the threshold voltage ($V_{\rm th}$). Through this sequence, we can implement $T_{\rm res}$, which is the duration of $V_{\rm res3,4}$. The value of $T_{\rm res}$ can be controlled by the current ($I_{\rm dg}$), which is related to the resistor ($R_{\rm dg}$) and to the calibrated voltage ($V_{\rm cal}$). To minimize the quiescent current, we used a large value of $R_{\rm dg}$ of 20 M$\Omega$, which was integrated into the chip. To determine whether the proposed harvester enters $\Phi_{\rm BF}$ or $\Phi_H$, we used a switch controller that consists of latched comparators, oscillators, a zero current

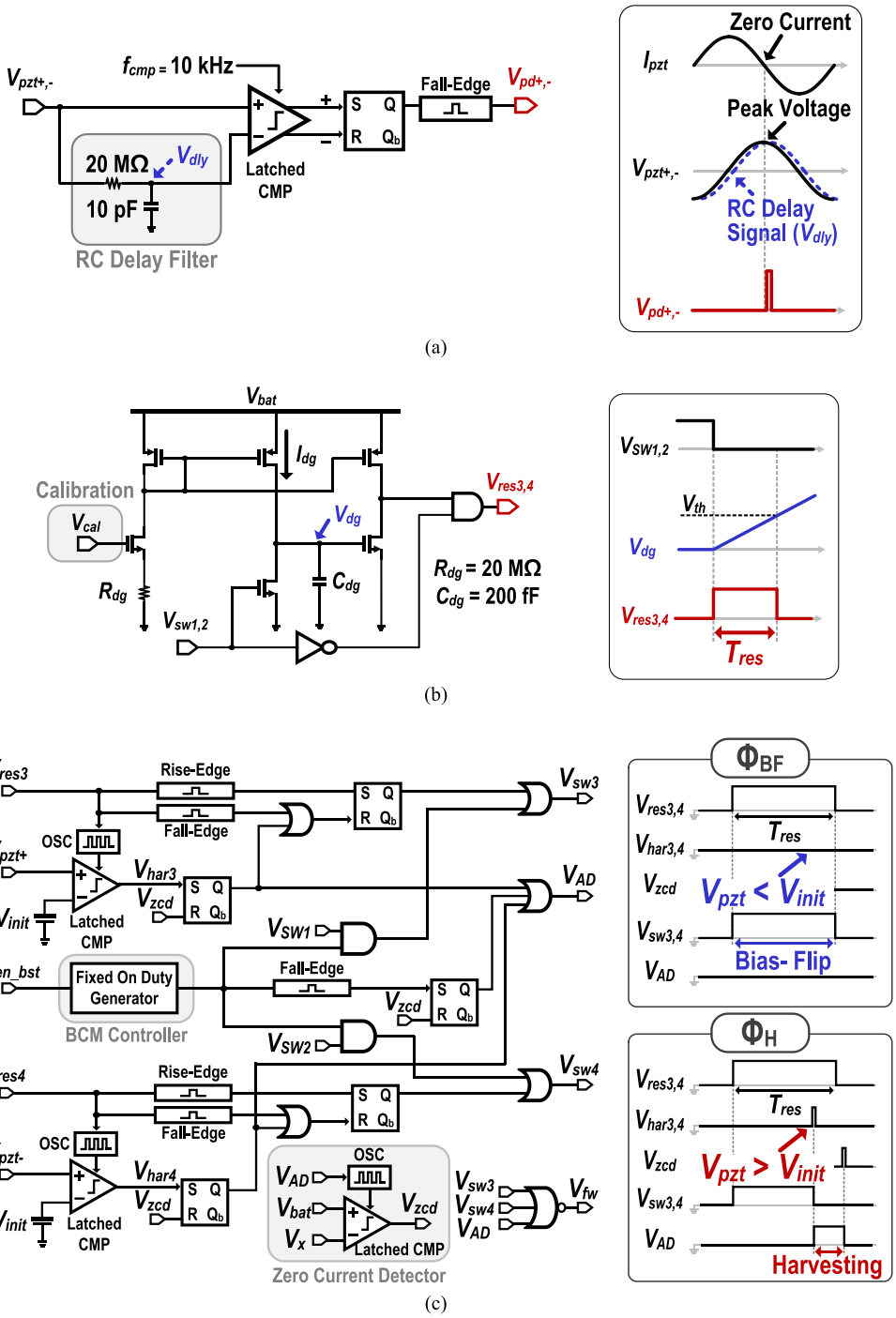


Fig. 10. Control block diagrams in detail. (a) Peak detector. (b) Duty generator. (c) Switch controller.

detector, and digital logic blocks, as shown in Fig. 10(c). If $V_{pzt+}$ (or $V_{pzt-}$) reaches $V_{init}$ during the on-time of $V_{res3}$ (or $V_{res4}$), a harvesting signal $V_{har3}$ (or $V_{har4}$) is generated to disable $V_{sw3}$ (or $V_{sw4}$). Then, the AD signal ($V_{AD}$) is enabled to start the harvesting, which continues until the zero current detect signal of $I_{ind}$ ($V_{zcd}$) is generated. Otherwise, $V_{har3}$ (or $V_{har4}$) is not generated to maintain the $LC$ resonance during $T_{res}$. To minimize the quiescent current of the switch controller, all the latched comparators only work during the period, in which comparison is needed. For the operation of BCM, we used a conventional controller that generates a fixed-on duty signal in pulse frequency modulation, which is enabled by the boost signal ($V_{en_bst}$). By adopting the simple control schemes, the proposed harvester can operate in both DPM and BCM, while consuming low quiescent current.

## V. Measurement Results

Fig. 11 shows that our energy harvester interface circuit [25] was implemented in a 0.18-$\mu$m BCD process with dimensions of 1.5 mm$^2$. Power switches and passive elements, such as resistors and capacitors, occupy the majority of the chip area. The active area of the control block is 0.22 mm$^2$. The chip was tested with a 680-$\mu$H inductor and a 20-nF commercial product piezoelectric device (Mide PPA-1001). The piezoelectric

TABLE I
PERFORMANCE COMPARISON

| | ISSCC 2010 [13] | JSSC 2014 [17] | ISSCC 2014 [23] | **This Work** |
|---|---|---|---|---|
| Energy Harvesting Sources | Piezoelectric Transducer | Piezoelectric Transducer | Piezoelectric Transducer & Thermoelectric Generator | **Piezoelectric Transducer & Thermoelectric Generator** |
| Piezoelectric Product | PiezoSystems, Inc | Mide V22B | Emulated Transformer | **Mide PPA-1001** |
| Harvesting Technique | Rectifier-less | Investment | Pile-up Resonance | **Double Pile-up Resonance** |
| Output Voltage | 2.7 – 3.8 V | 2.7 – 3.8 V | 2 – 4 V | **3 – 4 V** |
| Inductor | 150 µH | 330 µH | 10000 µH | **680 µH** |
| Idle Current | N / A | N / A | N / A | **240 nA** |
| Simultaneous Extraction | No | No | No | **Yes** |
| Boost Converter Efficiency | N / A | N / A | N / A | **75 % (at 450 µW)** |
| * Power Extraction Improvement (F.O.M) | ** 43 % | 351 % | ** 936 % | **1452 %** |

* F.O.M = Extracted output power (= $P_{out}$) × 100 / Maximum extracted power of ideal full-bridge rectifier (= $C_{pzt} \times f_{pzt} \times V_{pzt,oc}^2$) defined in [17]
** Re-calculation as F.O.M

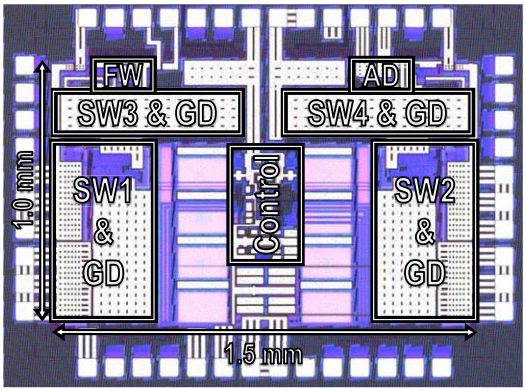


Fig. 11. Micrograph of the proposed energy harvesting chip.

device, with a clamper kit (Mide PPA-9001), was mounted on a mini shaker (Brüel & Kjær Type 4810). A function generator (Agilent 33120) and a power amplifier (Brüel & Kjær Type 2718) were used to control the frequency and the strength of the shaker's movement, respectively. To measure the performance under various conditions, both the TEG and the battery were modeled as a precision power supply device (Agilent N6761) that can support several power terminals. A 200-Ω resistor was used in series with TEG.

Fig. 12 shows the measured oscilloscope waveforms of the proposed energy harvester for various scenarios. For these measurements, $V_{\mathrm{pzt,oc}}$, $V_{\mathrm{bat}}$, and, $f_{\mathrm{pzt}}$ were 0.6 V, 4 V, and 140 Hz, respectively. Fig. 12(a) shows that the proposed harvester successfully increased the $V_{\mathrm{pzt}}$ to a peak-to-peak voltage ($V_{\mathrm{pzt,pp}}$) of 7 V, allowing the extraction of more electrical energy. In addition, by the time-multiplexing method, the harvester operated in both DPM and BCM to simultaneously extract energy from the PZT and the TEG, as shown in Fig. 12(b). Despite using the same operating conditions of PZT, $T_{\mathrm{har}}$ increased from 2 to 4 $\mu$s as $V_{\mathrm{teg}}$ was increased from 100 to 500 mV, respectively, as can be seen in Fig. 12(c) and (d).

Fig. 13 shows the measured graphs under various conditions. The comparison between theoretical output power and measured output power of the proposed harvester operating only in DPM is shown in Fig. 13(a). According to (13), the proposed harvester can theoretically obtain a value of 20 $\mu$W, when PZT only operates without TEG under the operating conditions that $V_{\mathrm{oc,pzt}}$, $C_{\mathrm{pzt}}$, and $f_{\mathrm{pzt}}$ are 0.6 V, 20 nF, and 140 Hz, respectively. However, the proposed harvester practically extracted the output power of 16 $\mu$W. This is because the theoretical output power is calculated without parasitic resistance of power switches, inductor, and controller power consumption. Under the same conditions, nevertheless, the proposed harvester leads to a 1452% power extraction improvement, compared with the FBR that can obtain a value of 1.1 $\mu$W, as was found in (6). Moreover, more extracted power was obtained as $V_{\mathrm{teg}}$ was increased. By increasing the operating frequency of BCM ($f_{\mathrm{bst}}$) up to 100 kHz, the harvester obtained the maximum output power of 450 $\mu$W with a peak efficiency of 75%, as shown in Fig. 13(b). Comparing each extracted power in Fig. 13(a) and (b), the measured power of BCM is much larger than that of DPM. This is because the operating frequency is quite different between them; the operating frequency of DPM and BCM are 140 Hz and 100 kHz, respectively. Maximum quiescent current was 240 nA at $V_{\mathrm{bat}} = 4$ V, as shown in Fig. 13(c).

Table I summarizes the performance of this chip in comparison with those of state-of-the art chips. Our harvester mainly operates in the range of output voltage from 3 to 4 V in order to achieve the better performance of power extraction. Among all other results reported recently, this paper achieved the best power extraction improvement of 1452%, using only with PZT. Moreover, the proposed harvester enables simultaneous energy

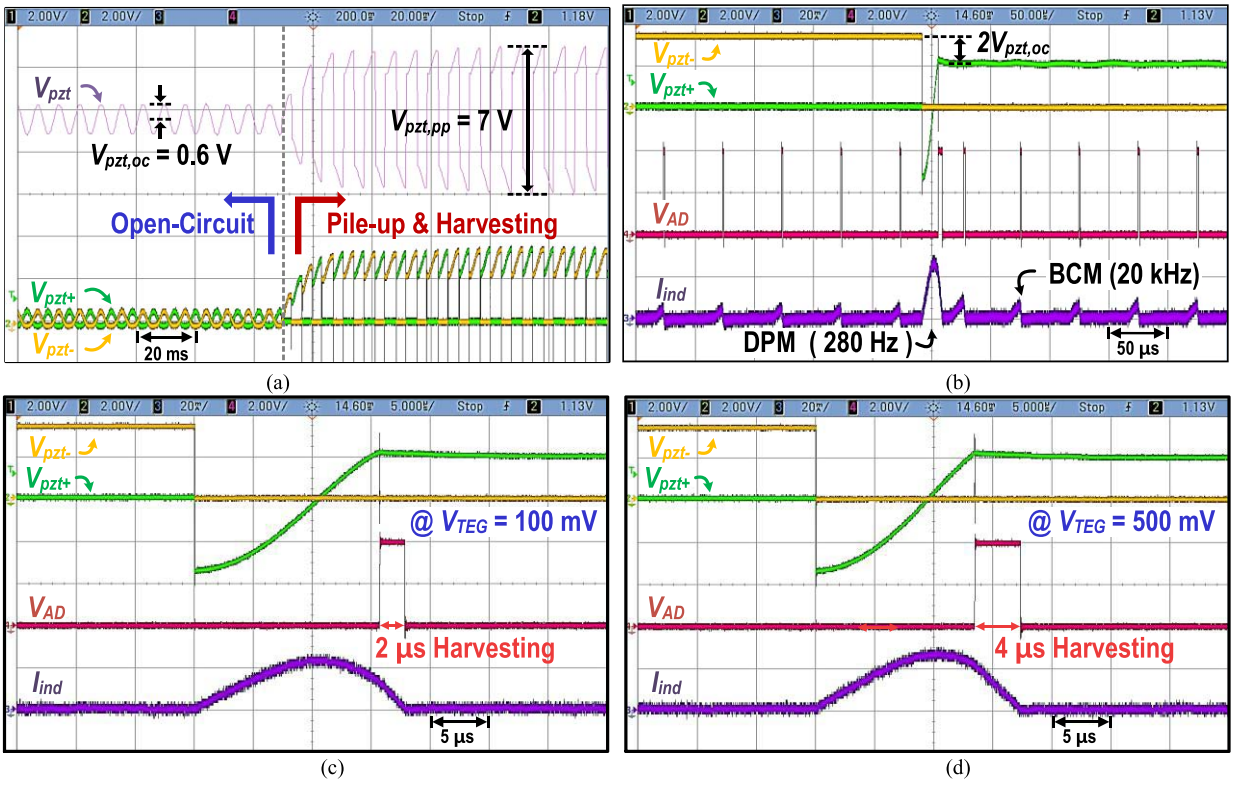


Fig. 12. Measured waveforms. (a) Startup. (b) Steady state. (c) Harvesting phase at $V_{\text{teg}} = 100$ mV. (d) Harvesting phase at $V_{\text{teg}} = 500$ mV.

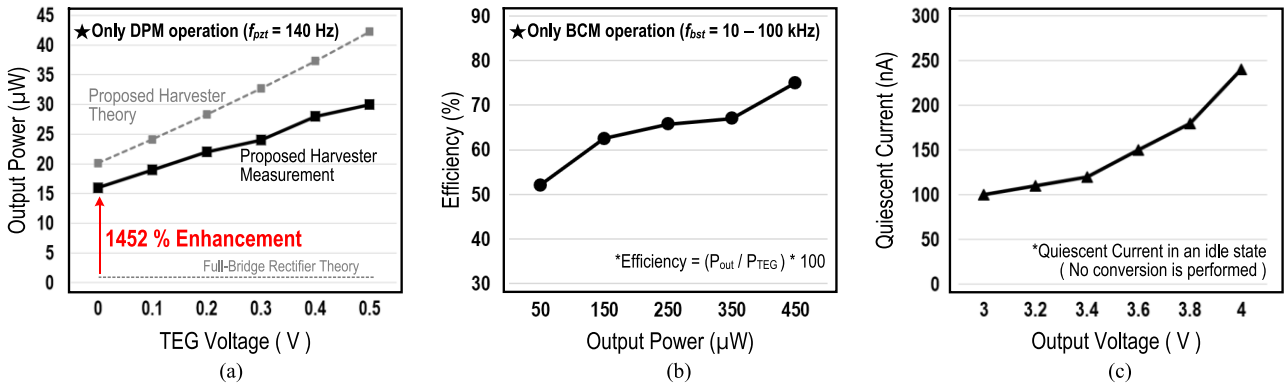


Fig. 13. Measured graphs. (a) Output power in DPM as $V_{\text{teg}}$. (b) Efficiency in BCM as $P_{\text{out}}$. (c) Quiescent current as $V_{\text{bat}}$.

extraction from both the PZT and TEG, while consuming a low quiescent current of 240 nA.

## VI. Conclusion

In this paper, a double pile-up resonance energy harvesting circuit that simultaneously extracts energy from PZT and TEG is presented. The proposed harvester improves power extraction by adopting a double pile-up technique; the proposed harvesting circuit operates while consuming sub-microampere quiescent current. In addition, by quantitatively analyzing previous approaches and this paper, it was sufficiently verified that the proposed structure can extract energy more than the other harvesters. The experimental results verify the validity of the proposed energy harvesting circuit. Therefore, the proposed energy harvester is thought to be the best candidate for a low-powered multiple energy source harvesting circuit.

## References

[1] R. J. M. Vullers, R. V. Schaijk, H. J. Visser, J. Penders, and C. V. Hoof, "Energy harvesting for autonomous wireless sensor networks," *IEEE Solid State Circuits Mag.*, vol. 2, no. 2, pp. 29–38, Feb. 2010.

[2] W. B. Heinzelman, A. P. Chandrakasan, and H. Balakrishnan, "An application-specific protocol architecture for wireless microsensor networks," *IEEE Trans. Wireless Commun.*, vol. 1, no. 4, pp. 660–670, Oct. 2002.

[3] J. C. Kwan and A. O. Fapojuwo, "Radio frequency energy harvesting and data rate optimization in wireless information and power transfer sensor networks," *IEEE Sensors J.*, vol. 17, no. 15, pp. 4862–4874, Aug. 2017.

[4] X. Liu and E. Sánchez-Sinencio, "An 86% efficiency 12 $\mu$W self-sustaining PV energy harvesting system with hysteresis regulation and time-domain MPPT for IOT smart nodes," *IEEE J. Solid-State Circuits*, vol. 50, no. 6, pp. 1424–1437, Jun. 2015.

[5] S. Bandyopadhyay and A. P. Chandrakasan, "Platform architecture for solar, thermal, and vibration energy combining with MPPT and single inductor," *IEEE J. Solid-State Circuits*, vol. 47, no. 9, pp. 2199–2215, Sep. 2012.

[6] Y. K. Ramadass and A. P. Chandrakasan, "An efficient piezoelectric energy harvesting interface circuit using a bias-flip rectifier and shared inductor," *IEEE J. Solid-State Circuits*, vol. 45, no. 1, pp. 189–204, Jan. 2010.
[7] G. K. Ottman, H. F. Hofmann, A. C. Bhatt, and G. A. Lesieutre, "Adaptive piezoelectric energy harvesting circuit for wireless remote power supply," *IEEE Trans. Power Electron.*, vol. 17, no. 5, pp. 669–676, Sep. 2002.
[8] S. Du, Y. Jia, C. D. Do, and A. A. Seshia, "An efficient SSHI interface with increased input range for piezoelectric energy harvesting under variable conditions," *IEEE J. Solid-State Circuits*, vol. 51, no. 11, pp. 2729–2742, Nov. 2016.
[9] A. Romani, M. Filippi, and M. Tartagni, "Micropower design of a fully autonomous energy harvesting circuit for arrays of piezoelectric transducers," *IEEE Trans. Power Electron.*, vol. 29, no. 2, pp. 729–739, Feb. 2014.
[10] X.-D. Do, H.-H. Nguyen, S.-K. Han, D. S. Ha, and S.-G. Lee, "A self-powered high-efficiency rectifier with automatic resetting of transducer capacitance in piezoelectric energy harvesting systems," *IEEE Trans. Very Large Scale Integr. (VLSI) Syst.*, vol. 23, no. 3, pp. 444–453, Mar. 2015.
[11] M. Shim, J. Kim, J. Jung, and C. Kim, "Self-powered 30 $\mu$W-to-10 mW piezoelectric energy-harvesting system with 9.09 ms/V maximum power point tracking time," in *IEEE Int. Solid-State Circuits Conf. (ISSCC) Dig. Tech. Papers*, Feb. 2014, pp. 406–407.
[12] J. Sankman and D. Ma, "A 12-$\mu$W to 1.1-mW AIM piezoelectric energy harvester for time-varying vibrations with 450-nA $I_Q$," *IEEE Trans. Power Electron.*, vol. 30, no. 2, pp. 632–643, Feb. 2015.
[13] D. Kwon and G. A. Rincon-Mora, "A single-inductor AC-DC piezoelectric energy-harvester/battery-charger IC converting $\pm$(0.35 to 1.2V) to (2.7 to 4.5V)," in *PIEEE Int. Solid-State Circuits Conf. (ISSCC) Dig. Tech. Papers*, Feb. 2010, pp. 494–495.
[14] S. Du, Y. Jia, and A. A. Seshia, "An efficient inductorless dynamically configured interface circuit for piezoelectric vibration energy harvesting," *IEEE Trans. Power Electron.*, vol. 32, no. 5, pp. 3595–3609, May 2017.
[15] D. A. Sanchez, J. Leicht, F. Hagedorn, E. Jodka, E. Fazel, and Y. Manoli, "A parallel-SSHI rectifier for piezoelectric energy harvesting of periodic and shock excitations," *IEEE J. Solid-State Circuits*, vol. 51, no. 12, pp. 2867–2879, Dec. 2016.
[16] S. Lu and F. Boussaid, "A highly efficient P-SSHI rectifier for piezoelectric energy harvesting," *IEEE Trans. Power Electron.*, vol. 30, no. 10, pp. 5364–5369, Oct. 2015.
[17] D. Kwon and G. A. Rincón-Mora, "A single-inductor 0.35 $\mu$m CMOS energy-investing piezoelectric harvester," *IEEE J. Solid-State Circuits*, vol. 49, no. 10, pp. 2277–2291, Oct. 2014.
[18] D. Guyomar, A. Badel, E. Lefeuvre, and C. Richard, "Toward energy harvesting using active materials and conversion improvement by nonlinear processing," *IEEE Trans. Ultrason., Ferroelect., Freq. Control*, vol. 52, no. 4, pp. 584–595, Apr. 2005.
[19] E. Lefeuvre, D. Audigier, C. Richard, and D. Guyomar, "Buck-boost converter for sensorless power optimization of piezoelectric energy harvester," *IEEE Trans. Power Electron.*, vol. 22, no. 5, pp. 2018–2025, Sep. 2007.
[20] N. J. Guilar, R. Amirtharajah, and P. J. Hurst, "A full-wave rectifier with integrated peak selection for multiple electrode piezoelectric energy harvesters," *IEEE J. Solid-State Circuits*, vol. 40, no. 1, pp. 240–246, Jan. 2009.
[21] T. Hehn *et al.*, "A fully autonomous integrated interface circuit for piezoelectric harvesters," *IEEE J. Solid-State Circuits*, vol. 47, no. 9, pp. 2185–2198, Sep. 2012.
[22] A. Badel, A. Benayad, E. Lefeuvre, L. LeBrun, C. Richard, and D. Guyomar, "Single crystals and nonlinear process for outstanding vibration-powered electrical generators," *IEEE Trans. Ultrason., Ferroelect., Freq. Control*, vol. 53, no. 4, pp. 673–684, Apr. 2006.
[23] Y.-S. Yuk *et al.*, "An energy pile-up resonance circuit extracting maximum 422% energy from piezoelectric material in a dual-source energy-harvesting interface," in *IEEE Int. Solid-State Circuits Conf. (ISSCC) Dig. Tech. Papers*, Feb. 2014, pp. 402–403.
[24] M. Dini, A. Romani, M. Filippi, and M. Tartagni, "A nanopower synchronous charge extractor IC for low-voltage piezoelectric energy harvesting with residual charge inversion," *IEEE Trans. Power Electron.*, vol. 31, no. 2, pp. 1263–1274, Feb. 2016.
[25] K.-S. Yoon, S.-W. Hong, J.-S. Bang, S.-H. Lee, S.-W. Choi, and G.-H. Cho, "A 1452-% power extraction improvement energy harvesting circuit with simultaneous energy extraction from a piezoelectric transducer and a thermoelectric generator," in *Proc. Symp. VLSI*, Jun. 2017, pp. 202–203.
[26] G. Tang, B. Yang, J.-Q. Liu, B. Xu, H.-Y. Zhu, and C.-S. Yang, "Development of high performance piezoelectric $d_{33}$ mode MEMS vibration energy harvester based on PMN-PT single crystal thick film," *Sens. Actuators A, Phys.*, vol. 205, pp. 150–155, Jan. 2014.
[27] S. S. Dessai and A. Dessai, "Design of piezoelectric-thermoelectric hybrid energy harvester for wireless sensor network," in *Proc. Int. Conf. Smart Electron. (ICSES)*, May 2016, pp. 78–81.
[28] P. D. Mitcheson, "Energy harvesting for human wearable and implantable bio-sensors," in *Proc. IEEE Eng. Med. Biol. Soc. Conf.*, Jan. 2010, pp. 3432–3436.
[29] Linear Technology. (2013). *DC2080A*. [Online]. Available: http://www.linear.com/docs/43511
[30] Linear Technology. (2013). *DC2042A*. [Online]. Available: http://www.linear.com/docs/43514

**Kye-Seok Yoon** (S'17) received the B.S. degree in electrical engineering from Korea University, Seoul, South Korea, in 2012, and the M.S. degree in electrical engineering from the Korea Advanced Institute of Science and Technology, Daejeon, South Korea, in 2014, where he is currently pursuing the Ph.D. degree with the School of Electrical Engineering.

His current research interests include analog integrated circuit design, including the design and modeling of power management IC, low-dropout regulator, energy harvesting circuit, and wireless power transfer system.

**Sung-Wan Hong** received the B.S. degree in electrical engineering from Korea University, Seoul, South Korea, in 2009, and the M.S. and Ph.D. degrees in electrical engineering from the Korea Advanced Institute of Science and Technology, Daejeon, South Korea, in 2011 and 2014, respectively.

In 2014, he joined Samsung Electronics Ltd., Suwon, South Korea. Since 2017, he has been an Assistant Professor with the Department of Electronics Engineering, Sookmyung Women's University, Seoul. His current research interests include the design of analog integrated circuits such as power management IC, high-speed buffer amplifier, wireless power transfer, energy harvesting, envelope modulator, and touch readout IC.

**Gyu-Hyeong Cho** (S'76–M'80–SM'11–F'16) received the B.S. degree in electrical engineering from Hanyang University, Seoul, South Korea, and the M.S. and Ph.D. degrees in electrical engineering from the Korea Advanced Institute of Science and Technology (KAIST), Daejeon, South Korea, in 1975, 1977, and 1981, respectively.

During 1982–1983, he was with the Westinghouse research and Development Center, Pittsburgh, PA, USA. In 1984, he joined the Department of Electrical Engineering, KAIST, where he has been a Full Professor since 1991. He has authored one book on advanced electronic circuits and authored or coauthored over 200 technical papers and 80 patents. His was involved in the area of power electronics until the late 1990s and focused on soft switching converters and high-power converters. Later, he shifted to analog integrated circuit design. His current research interests include power management ICs, Class-D amplifiers, touch sensors and drivers for AMOLED and LCD flat panel displays, and biosensors and wireless power transfer systems.

Prof. Cho received the Outstanding Teaching Award from KAIST. He served as a member of the ISSCC International Technical Program Committee, and is currently an Associate Editor of the IEEE JOURNAL OF SOLID-STATE CIRCUITS. At the ISSCC 60th Anniversary in 2013, he was awarded the ISSCC Author-Recognition Award as one of the top 16 contributors of the conference during last 60 years in ISSCC.